20 May 2002

PHYSICS LETTERS A

ELSEVIER

Physics Letters A 297 (2002) 376–386

www.elsevier.com/locate/pla

Self-affine nature of the stress-strain behavior of an elastic fractal network

Alexander S. Balankin *, Orlando Susarrey H., Guillermo Urriolagoitia C., Luis H. Hernández

SEPI-ESIME, Ed. 5, 3er Piso, Instituto Politécnico Nacional, México, D.F. 07738, Mexico

Received 8 October 2001; received in revised form 27 November 2001; accepted 1 April 2002

Communicated by A.R. Bishop

Abstract

The stress-strain behavior of fractal networks possesses self-affine scaling associated with statistical scale invariance of damage patterns. We found that the damage part of stress-strain curve of fractal network and the corresponding rupture line are characterized by the same scaling (Hurst) exponent, H, which is not universal, rather it depends on the network fractal dimension as $H = D_B - 1$. Furthermore, the same exponent governs the changes in the stress-strain behavior as the strain rate increases. These results were reproduced by Monte Carlo simulations using a fractal version of fiber bundle model. © 2002 Published by Elsevier Science B.V.

PACS: 46.50.+j; 46.30.Nz; 47.53.+n; 61.43 Hv

Keywords: Fractal network; Fracture; Self-affine scaling

1. Introduction

Mechanical behaviour of heterogeneous materials has attracted scientific and industrial interest for many years [1–3]. An important class of heterogeneous materials with complex mechanical behaviour is the stochastic fiber networks. Instead of a single crack growth, the failure of a fiber network often occurs as the culmination of progressive damage, involving complex interactions between multiple defects and growing micro-cracks [1–8]. In such a case, the stress-strain curve, $\sigma(\varepsilon)$, displays a stochastic behavior, which is characteristic of many disordered fibrous materials, such as fiber-reinforced composites and various kinds of paper [1,8].

Most of the theoretical investigations in this field rely on the computer simulation of lattice models, where the fiber network is represented by an Euclidean spring (beam) network, and disorder is captured either by random dilution or by assigning uncorrelated (random) failure thresholds to the springs [4–7]. In fact, however, whether the material in question is a paper, a glass fiber material, or a stochastically oriented fiber composite, the structure of network is not random, but it possess a long-range correlation associated with statistical scale invariance within a bounded interval of length scale [9,10]. In this way, a stochastic fiber network can be treated as a fractal (or, generally, multi-

* Corresponding author.
E-mail address: abalankin@sni.conacyt.mx (A.S. Balankin).

0375-9601/02/$ – see front matter
PII: S0375-9601(02)00427-9

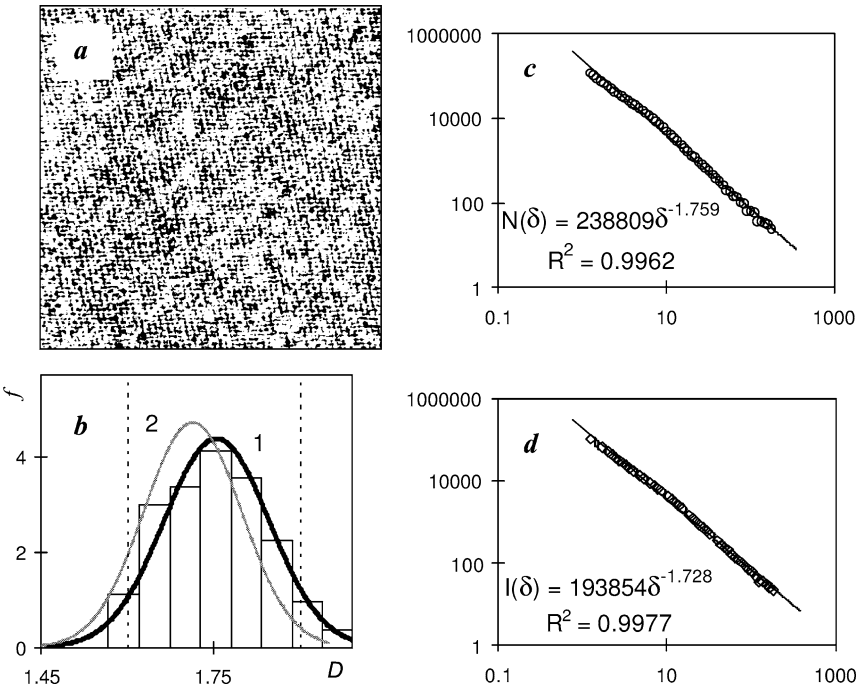

Fig. 1. (a) Black-and-white image of the toilet paper structure; (c), (d) the fractal graphs of image (a); and (b) statistical distributions of (1) the box-counting (significance level $p = 0.6911$) and (2) information ($p = 0.584$) dimensions (bins—experimental data, solid curves—fitting by a normal distribution).

fractal), characterized by the fractional metric (fractal) dimension D, which governs the mass–density correlations in the network [9] and its mechanical properties [2].

The interaction among multiple defects in a fractal structure with several characteristic scales and its effect on the mechanical behavior of composite materials present a considerable challenge in modeling and prediction of material failure. Unfortunately, models based on the Euclidean geometry of fiber network cannot capture the effect of long-range correlations associated with the fractal nature of a wide class of fiber networks. In this Letter, we specifically study the effect of fractal structure on the mechanical behavior and the scaling properties of damage patterns in fractal fiber networks.

2. Experimental details

Classical example of fractal fiber network is a paper [10,11]. The fiber distribution in a paper is not random, but possesses long-range mass density correlations of a power-law type [9]. The later indicates the (multi)-fractal nature of the paper structure [12]. In this way, different papers are characterized by diversity of fractal dimensions of fiber network [9,12]. This makes a paper an ideal model for purpose of present studies.

Different kinds of paper also possess diverse types of stress-strain behavior and different failure features [8,12–14]. Specifically, many papers exhibit elasto-plastic behavior, where plastic deformations are associated with the displacements between fibers [13]. For the present study, we selected a toilet paper, which displays quasi-linear elastic behavior up to failure threshold, with minimum inter-fiber displacements [8,13]. The thickness and areal density of this paper display considerable variations in accordance with a normal distribution and a mean of $h = 0.11 \pm 0.06$ mm and $\rho = 36.8 \pm 0.3\ \mathrm{g\,m^{-2}}$, respectively.

To study the fractal characteristics of paper structure, the gray scale optic micrographs of paper were scanned with 600×600 pixel resolution. Then, the gray scale photos were converted in black-and-white images (see Fig. 1(a)), using the histogram median (obtained with use the SCION IMAGE@ software [15])

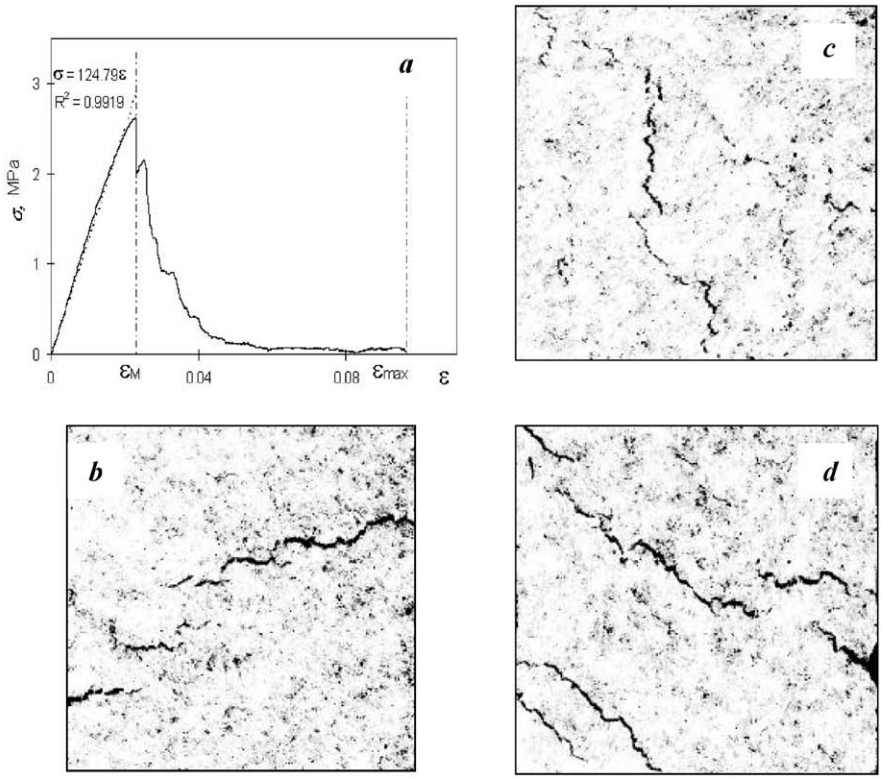

Fig. 2. (a) Engineering strain-stress curve of toilet paper and (b)–(d) damage patterns in paper sheets loaded: (b) parallel to the machine direction, (c) perpendicular to the machine direction and (d) in the direction inclined 45° with respect to the machine direction of paper.

as a threshold value. The box-counting, D_B, and the information, D_I, dimensions were determined by using the commercial software BENOIT 1.2 [16].

Several mechanical tests were carried out on a 4505 INSTRON testing machine. The tested paper sheets of length $L = 10$ cm and width $W = 5$ cm were uniaxially loaded with deformation rate controlled by the grip displacement speeds (du/dt) of 0.5, 1, 2.5, 5, 10, and 100 mm min^{-1}. In all cases, the stress-strain measurement rate was hold at 50 points s^{-1}. At least, 30 paper sheets were tested for each displacement speed (the deformation rate $\dot{\varepsilon} = L^{-1}\,du/dt$ was 0.005, 0.01, 0.025, 0.05, 0.1, and 1 min^{-1}, respectively). Some additional experiments were carried out with paper sheets of length $L = 20$ cm and width $W = 10$ cm. A characteristic engineer stress-strain curve of toilet paper is shown in Fig. 2(a).

The scaling properties of each rupture line (see Fig. 3(a)–(c)), as well as each stress-strain curve (Fig. 3(d)), were studied by five different statistical methods adopted in the BENOIT 1.2 software [16]: the variogram, roughness-length, wavelets, power-spectrum and rescaled-range (R/S) analysis. For this purpose, the fractured sheets were scanned in black and white in the BMP format (Fig. 3(b)) with a 600×600 dpi^2 resolution. Then, the rupture lines were plotted using the SCION IMAGE software [15] as single-valued functions $z(x)$ in the XLS format (see Fig. 3(c)). All statistical data was handled with @RISK software [17], thus was found the best statistical fitting using chi-squared, Kolmogorov–Smirnov and Anderson–Darling statistics.

3. Experimental results

First of all, we note that the box-counting (see Fig. 1(c)) and information (see Fig. 1(d)) dimensions of paper structure are not constants, rather they change from sample to sample (30 micrographs of toilet

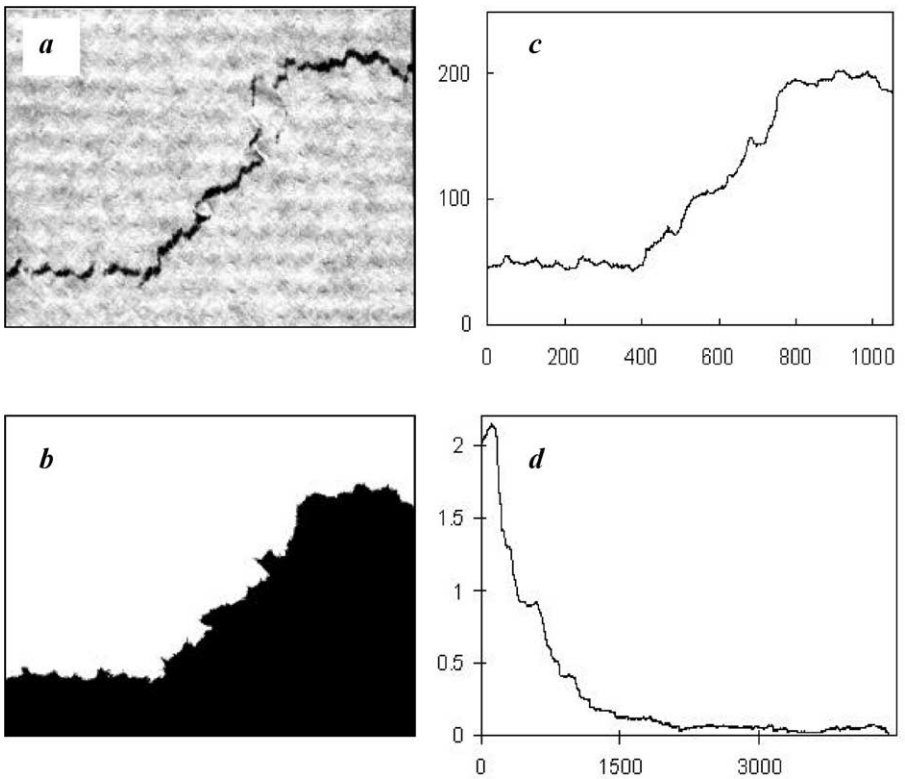

Fig. 3. (a) Damage and (b) rupture line images, and graphs $z(x)$ of: (c) rupture line and (d) damage part of stress-strain curve.

paper were analyzed) in accordance with a normal distribution (see Fig. 1(b)). These variations are larger than a statistical error of dimension estimation and can be attributed to the variations in the paper structure (associated also with the already mentioned above variances in the paper thickness and areal density). In all cases, we found that the general inequality for multifractals, $D_B > D_I$, is hold (see Fig. 1(b)–(d)). However, the difference $D_B - D_I$ is quite small, such that $D_B - D_I < \sigma[0.5(D_B + D_I)]$, where $\sigma[\cdots]$ is the standard deviation of data for a set of studied images. Therefore, in accordance to the criterion [18], the structure of toilet paper can be treated as a statistically self-similar. At the same time, the slight changes in the slopes of graphs in Fig. 1(c),(d) probably indicate the self-affine nature of fiber network (see Ref. [19]), caused by the fiber alignment in the machine direction.

Most papers possess anisotropic mechanical properties associated with a preferred fiber orientation in the machine direction [11]. So, first, we have studied the mechanical behavior of paper under uniaxial tension in different directions. Toilet paper displays a linear elastic behavior up to the tensile stress σ_M (see Fig. 2(a)) for any direction. This indicates that an individual fiber is linearly elastic up to its rupture threshold. We also found that the Young modulus, the ultimate strength, and the maximum strain (see Fig. 2(a)) continuously decrease as the loading direction changes from the paper machine direction to the transversal direction. Specifically, in experiments with a deformation rate of 0.05 min^{-1}, we find that in the machine direction $E = 166 \pm 20$ MPa, $\sigma_{max} = 2.7 \pm 0.4$ MPa and $\varepsilon_{max} = 2.3 \pm 0.3\%$, whereas in the transversal direction $E = 101 \pm 20$ MPa, $\sigma_{max} = 1.5 \pm 0.5$ MPa, and $\varepsilon_{max} = 2.0 \pm 0.3\%$. The anisotropy of paper structure is also reflected in the anisotropy of damage patterns in paper sheets loaded in different directions (see Fig. 2(b)–(d)).

The failure of toilet paper occurs as the culmination of progressive damage, involving complex interactions among multiple defects and growing micro-cracks (see Figs. 2(b)–(d) and 3(a)). Different fibers achieve

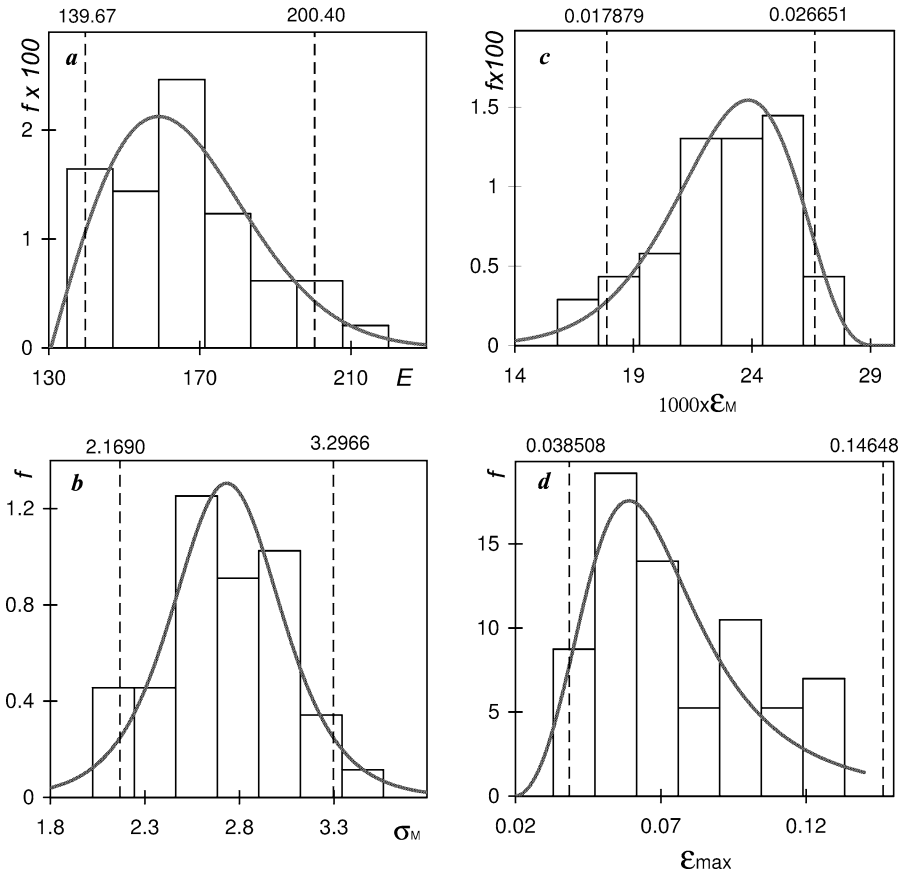

Fig. 4. Statistical distributions of (a) Young modulus ($p = 0.9029$), (b) ultimate tensile strength ($p = 0.6356$), (c) deformation threshold ($p = 0.6356$) and (c) maximum strain ($p = 0.8245$) of toilet paper tested at a strain rate of 0.001 min^{-1}.

rupture thresholds at different deformations, ε_i, because of the difference in the fiber tortuosity. When one or more fibers fail, their loads are transferred to other surviving fibers, which achieve thresholds at larger deformations. As a result, the stress-strain curve displays a stochastic behavior (see Figs. 2(a) and 3(d)). We note that first fail fibers which are aligned in the paper machine direction, independently on the direction of uniaxial tension (see Fig. 2(b)–(d)). However, the characteristic form of the stress-strain curve (see Fig. 2(a)) maintains the same for any direction of loading. So, all results reported below correspond to the uniaxial tension in the machine direction of toilet paper.

Accordingly, we have observed that all the stress-strain curve parameters (Young modulus E, ultimate tensile stress σ_{M}, deformation threshold ε_{M}, maximum deformation ε_{max}, fracture energy $U_F = \int_{\varepsilon_{\text{M}}}^{\varepsilon_{\text{max}}} \sigma \, d\varepsilon$, and deformation range of damage ($\delta = \varepsilon_{\text{max}} - \varepsilon_{\text{M}}$) vary from sample to sample, following a statistical distribution (see Figs. 4–6). Specifically, we found that δ ($\dot{\varepsilon} = \text{const}$) displays a normal distribution (Fig. 6(a)), while data at all deformation rates are best fitted with an inverse-Gauss distribution (Fig. 6(c)). Young modulus data conform a Raleigh distribution; σ_{M} data is best fitted with a logistic distribution (Fig. 4(b)); ε_{M} exhibit a beta-general distribution (Fig. 4(c)); whereas U_{F} and ε_{max} are best fitted with a log-logistic distribution (see Figs. 4(d) and 5(a)).

The means and standard deviations for these distributions are functions of the strain deformation rate, ε (see, for example, Figs. 5(b) and 6(a),(b). Specifically, we found that

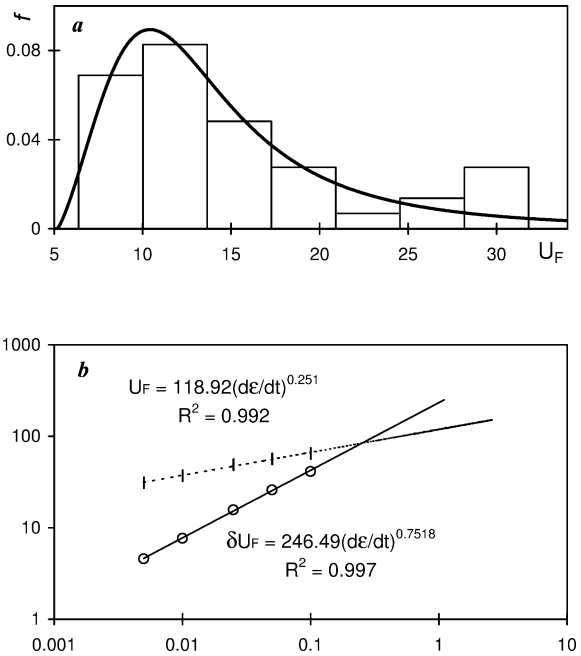

Fig. 5. (a) Statistical distributions of fracture energy and (b) graphs of U_F and $s(U_F)$ versus strain rate.

$$E = 245\dot{\varepsilon}^{0.087}\ \text{MPa}, \qquad \sigma_M = 2.89\dot{\varepsilon}^{0.0085}\ \text{MPa},$$
$$\varepsilon_M = 0.0171\dot{\varepsilon}^{-0.0661}, \qquad \varepsilon_{max} = 0.16\dot{\varepsilon}^{0.17},$$
$$\delta = 0.1454\dot{\varepsilon}^{0.2321}, \qquad s(\delta) = 0.6852\dot{\varepsilon}^{0.7242},$$
$$U_F = 121\dot{\varepsilon}^{0.251}, \qquad s(U_F) = 252\dot{\varepsilon}^{0.752}, \qquad (1)$$

in the range $0.005 \leqslant \dot{\varepsilon} \leqslant 0.1\ \text{min}^{-1}$ ($s(\cdots)$ means the standard deviation). These relations fail when the strain rate is $\dot{\varepsilon} = 1\ \text{min}^{-1}$. The reason for this change may be the change in the failure regime [20], which will be studied in a future work.

Fig. 7(a)–(d) show the fractal graphs for the stress-strain curve and corresponding rupture line in toilet paper (see Fig. 3(c),(d)), obtained by four methods mentioned above. From the experimental data, we note that all methods lead to the same value of the roughness exponent $\alpha = H$ for a given stress-strain curve and the corresponding rupture line (see Fig. 8). Test on the anomalous crack roughening (see [14,21]) has shown that the rupture lines in toilet paper (see Fig. 3(b),(c)) are statistically auto-affine within a wide but bounded range of length scale.

At the same time, we find that the scaling exponent is not a universal one; rather it changes from sample

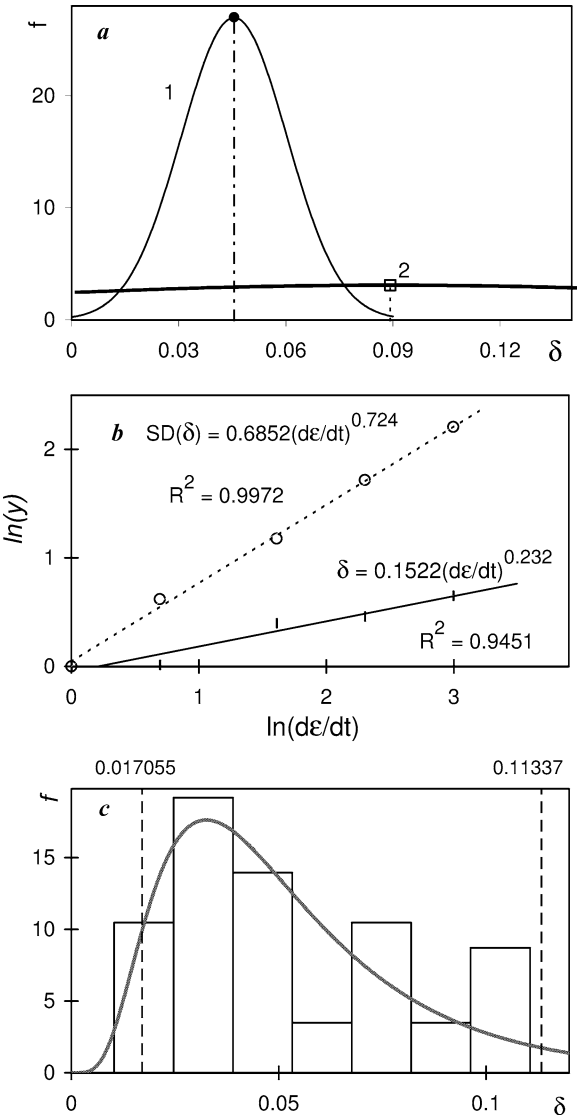

Fig. 6. (a) Statistical distributions of δ for specimens tested with a strain rate of (1) 0.0005 min^{-1} and (2) 0.1 min^{-1}; (b) δ and $s(\delta)$ versus strain rate graphs; and (c) statistical distribution of δ for tests with different stain rates ($p = 0.8245$).

to sample in accordance with a normal distribution (Figs. 8 and 9). These variations are larger than statistical errors within a sample and they might be attributed to the sample-to-sample variation of the network structure (see Fig. 1(b)). On the other hand, we note that the mean value of $\alpha = H$ is independent on the strain rate (see Fig. 9(a)).

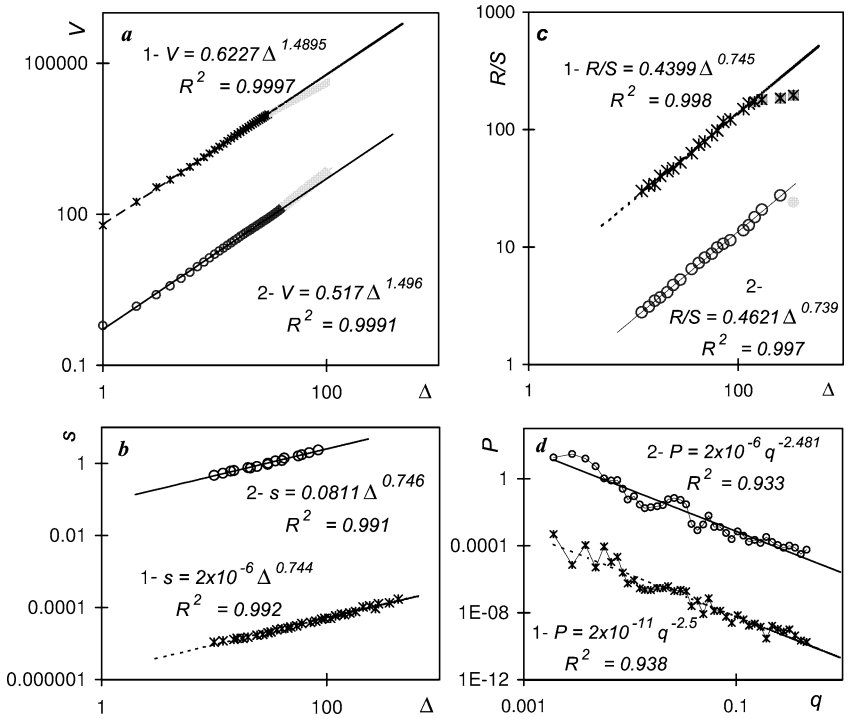

Fig. 7. (a)–(d) Fractal graphs of (1) the stress-strain curve, and (2) the corresponding rupture line for toilet paper (see Fig. 3(c) and (d)) obtained by (a) the variogram, (b) the roughness-length, (c) the rescaled range, and (d) the power-spectrum methods. Notice that in graphs (a) and (b) curves have been shifted vertically.

The data in Figs. 6–9 suggest that the stress-strain curve has a self-affine invariance, i.e.,

$$\sigma(\lambda\varepsilon) = \lambda^{-\alpha}\sigma(\varepsilon), \quad \text{with } \alpha = H, \tag{2}$$

where H is the rupture line roughness (Hurst) exponent, $\lambda > 0$ is a constant, $\varepsilon_{\mathrm{M}} < \varepsilon$, $\lambda\varepsilon < \varepsilon_{\max}$. Furthermore, we speculate that the experimental relations (1) may be cast in the form

$$\delta \propto U_{\mathrm{F}} \propto \dot{\varepsilon}^{1-H}, \qquad s(\delta) \propto s(U_{\mathrm{F}})\dot{\varepsilon} \propto \dot{\varepsilon}^{H}, \tag{3}$$

i.e., the failure dynamics is governed by the same Hurst exponent, which depends on the network structure (see also [8,12,22]).

To verify this assumption, a set of experiments at each deformation rate was divided in two subsets, associated with specimens with the lowest and the highest values of H. So, we obtain two sets of data with different means $H = \alpha = 0.645$ and $H = \alpha = 0.848$ (see Fig. 10(a)). One may expect that these sets correspond to different sets of networks with a different fractal dimension (see Fig. 10(b)), which were obtained by dividing the data shown in Fig. 1(b) in two sets. For specimens selected accordingly to corresponding values of H (see Fig. 9(a)), the means and the standard deviations of δ scale as $\delta \propto \dot{\varepsilon}^{0.367}$, $s(\delta) \propto \dot{\varepsilon}^{0.639}$ and $\delta \propto \dot{\varepsilon}^{0.157}$, $s(\delta) \propto \dot{\varepsilon}^{0.841}$ (see Fig. 10(c),(d)). The later is in good agreement with relations (3).

4. Fractal damage model

The observed failure behavior may be understood on the basis of a fractal damage model. The system under consideration is composed on N fibers, formed a two-dimensional fractal (probably, self-affine) network. The elastic energy function of the network formed by N elastic fibers can be represented as $U = 0.5E(N)\varepsilon^2$, where $E(N) = E_0 N(\varepsilon)$ is the elastic modulus of the network, E_0 is the fiber elastic modulus, and $N(\varepsilon)$ is a strictly decreasing continuous function of strain ε (N decreases every time as one or more

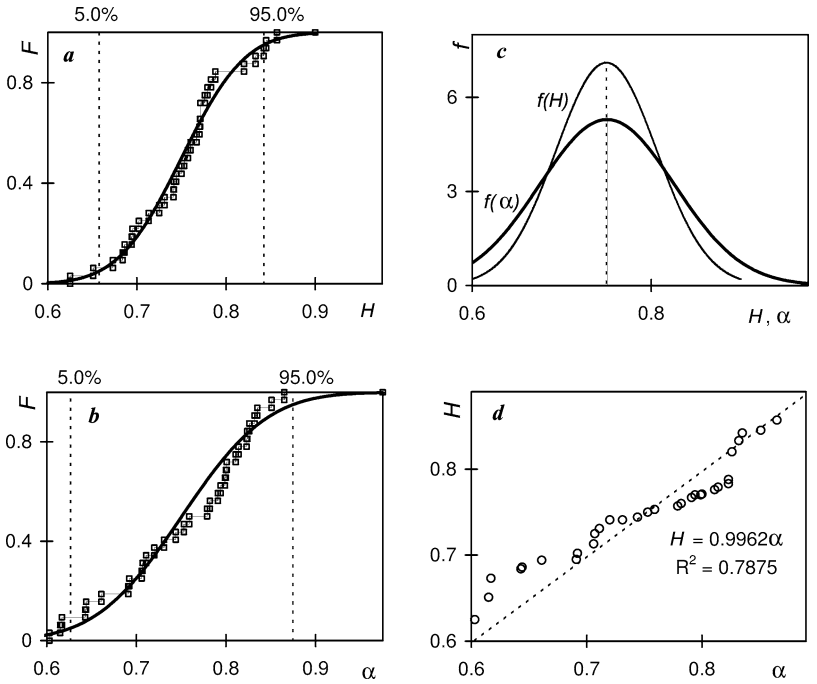

Fig. 8. Statistical distributions of: (a), (c) crack roughness exponent and (b), (c) stress-strain scaling exponent (solid lines—fitting by normal distribution); and (d) H versus α graph, for tests with a deformation rate $\dot{\varepsilon} = 0.01\ \text{min}^{-1}$.

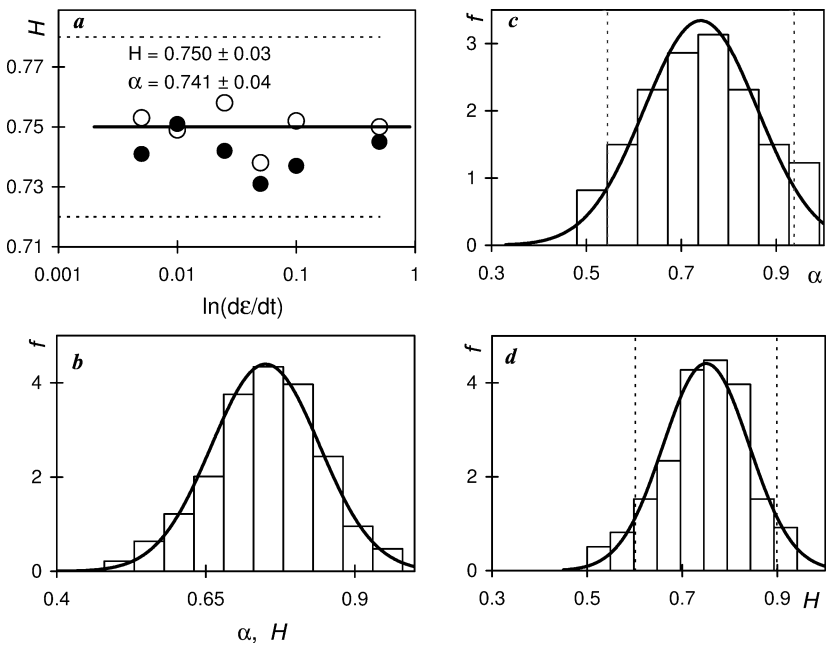

Fig. 9. (a) Graph of the mean value of H versus strain rate, and statistical distributions of complete sets of data for (b) scaling exponent (H and α) ($p = 0.9673$), (c) α ($p = 0.9631$) and (d) H ($p = 0.7622$) fitted by normal distribution (solid lines).

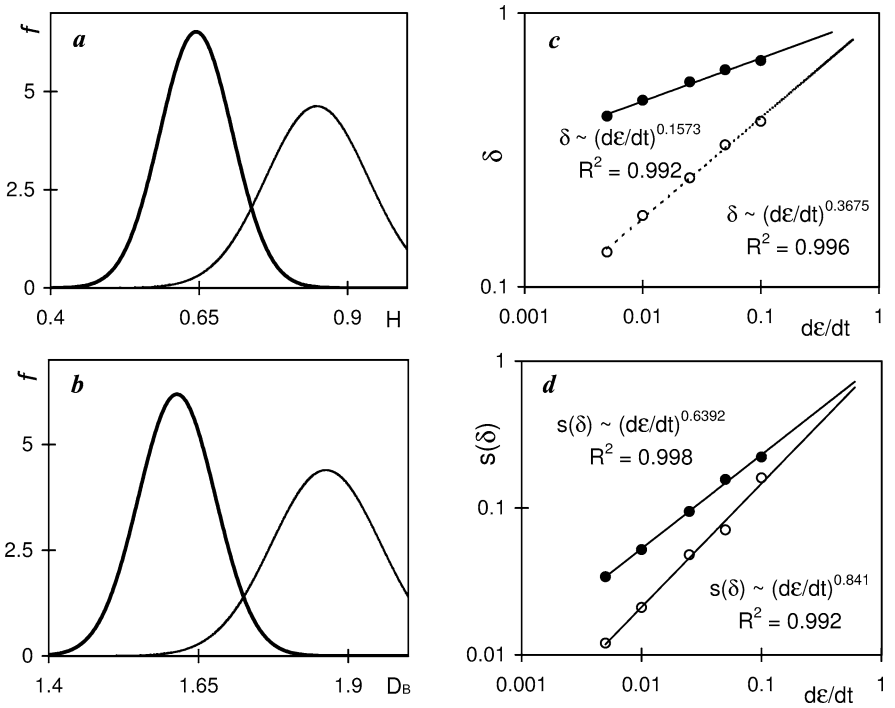

Fig. 10. Statistical distributions of (a) $H = \alpha$ and (b) D_F for two subsets of tested specimens; and graphs of (c) δ and (d) $s(\delta)$ versus strain rate for these subsets.

fibers fails) obeying the following properties:

$$N(\varepsilon \leqslant \varepsilon_1 < \varepsilon_M) = N_0,$$

$$N(\varepsilon_{max}) = 0 \quad \text{and} \quad \frac{dN}{d\varepsilon} \cong 0, \tag{4}$$

where the symbol "$\cong$" denotes "equal with exception of a Lebesgue set of zero-measure"; furthermore $dN/d\varepsilon = \infty$, when $\varepsilon = \varepsilon_i$, $i = 1, 2, \ldots, N$, where ε_i is the failure strain of the ith-fiber, which is a function of the strain rate (see Eq. (1)). The simplest steep-wise function which satisfies these conditions is $N(\varepsilon_i < \varepsilon < \varepsilon_{i+1}) = \text{const}$, $N(\varepsilon_i) = N_0[1 - (\varepsilon_i/\varepsilon_{max})^\gamma]$, where $\gamma \geqslant 0$ and $0 < \varepsilon_1 \leqslant \varepsilon_2 \leqslant \cdots < \varepsilon_N = \varepsilon_{max}$. Furthermore, one may expect that the set of critical deformations $\{\varepsilon_i\}$ is a Cantor-like set, its fractal dimension is determined by the fractal dimension of the fiber structure, e.g., $D_C = D_B - 1$ [10]. So, $N(\varepsilon_i)$ of an elastic fractal network can be modeled by the Devil's staircase [10] associated with the Cantor set of fractal dimension D_C.

Under these assumptions, $N(\varepsilon > \varepsilon_1)$ exhibits a statistical self-affine invariance, i.e.,

$$N(\lambda\varepsilon) = \lambda^{-\eta} N(\varepsilon), \tag{5}$$

where $\lambda > 0$, $\varepsilon_1 < \varepsilon$, $\lambda\varepsilon < \varepsilon_{max}$, $\eta = D_B$. Using the properties (3) of the Devil's staircase [10,23] and conventional thermodynamic assumptions [24], it is easy to derive the constitutive equation for an elastic (multi)-fractal network $\sigma = \frac{\partial U}{\partial \varepsilon} \cong E(N(\varepsilon))\varepsilon = E_0 N(\varepsilon)\varepsilon \propto \sigma^{-\alpha}$, which obeys a self-affine scaling (2) with $\alpha = D_B - 1 = D_C$, within the interval $\varepsilon_1 < \varepsilon$, $\lambda\varepsilon < \varepsilon_{max}$.

On the other hand, under the assumption that the rupture fractal dimension D_R is determined by the fractal dimension of fiber network, i.e., $D_R = 3 - D_B$ [12], we can expect that

$$H = 2 - D_R = D_B - 1 = D_C = \alpha, \tag{6}$$

in agreement with experimental observations (compare data from Figs. 8, 10 and 1(b)). Accordingly, relations (3) may be represented in the form of uncertainty

relations

$$s(\tau_F)U_F = C_1 = 85 \pm 35 \text{ mJ min},$$
$$\tau_F s(U_F) = C_2 = 38 \pm 15 \text{ mJ min}, \quad (7)$$

where $\tau_F = \delta/\dot{\varepsilon}$ is the time-to-fracture. Notice that these relations are similar to the energy-time uncertainty relation in quantum mechanics.

5. Monte Carlo simulations

To get a better insight into the dynamic properties of the fractal damage model, we explore the probabilistic nature of fiber failures using a variation of the well-known fiber bundle model, which was advanced in [5–7]. In fiber bundle models a set of fibers is arranged in parallel, each one has a statistically distributed strength. The fiber network is loaded parallel to the fibers direction, and the fibers fail if the load on them exceeds their threshold value. Once the fibers begin to fail, one can choose among several load transfer rules. In the simplest case of global load transfer, after fiber failure, the load is transferred equally to all remaining intact fibers. At the other extreme, one finds the local load sharing fiber bundle model [4–8], where the load borne by failing elements is transferred to their nearest neighbors. As it was pointed above, an important fraction of stress is redistributed to other intact fibers which are not localized in the neighborhood to the failed ones, nevertheless maintaining stress concentration around the broken fibers. So, actual stress redistribution in fiber network should be modeled by somewhat between the global and local load sharing models. One can expect that in a fractal network, the stress redistribution is governed by a power law

$$\sigma_{add} \propto r^{-\beta}, \quad (8)$$

where σ_{add} is the stress increase on a fiber at distance r from the failed fiber.

The system under consideration is composed of N fibers, assembled in parallel on a two dimensional square lattice of side length $L = \sqrt{N}$. To model a fractal structure of fiber network, we assume that the distribution of critical strains (ε_I) satisfies relations (5), where D_B is the fractal dimension of network, and the local stresses follow constitutive relation $\sigma = E_0\varepsilon$, where E_0 conforms an inverse-Gauss distribution. To capture the effect of stress-strain rate, we also assume that the Young modulus and the threshold stress of each fiber are power law functions (1) of strain rate.

A fiber fails when the load acting on it exceeds a threshold value. When a fiber fails, its load is transferred to other surviving fibers in the network, according to a specific transfer rule (8). So, during the simulation, the local stresses varied widely due to local density variations and fluctuations in the local stress transfer. As a result, instead of a single crack growth, the failure occurs as the culmination of progressive damage from multiple cracks.

Monte Carlo simulations also shown that the failure process starts from the lowest (one-fiber) level, when the network strain achieves a minimum critical value. Afterwards, the damage propagates from level to level due to failures of fiber groups (fibers with the same threshold deformation) with the consequent load redistribution (8). Accordingly, the cumulative distribution function of braked fibers, $F(\varepsilon_1 < \varepsilon < \varepsilon_M)$, is an increasing Devil's staircase associated with the Cantor set of dimension $D_C = D_B - 1$, such that $F(\varepsilon < \varepsilon_1) = 0$ and $F(\varepsilon \geqslant \varepsilon_M) = 1$. The macroscopic engineer stress behaves as $\sigma = E_0[1 - F(\varepsilon)]\varepsilon$. The network fails when the failure process envelops the entire network. The time the time-to-failure τ_F is defined as

$$\tau_F = \frac{\dot{\varepsilon}}{\varepsilon_M} = \frac{\dot{\varepsilon}}{\delta}. \quad (9)$$

Results of Monte Carlo simulations with $0.5 \leqslant \beta \leqslant 2$ reproduce relations (2), (3) and (6), (7), where $\alpha = D_B - 1$ and the constants C_1 and C_2 are dependent on the stress-transfer parameter β, as well on the D_B.

Detailed analysis of Monte Carlo simulations will be published elsewhere.

6. Conclusions

The failure behavior of a fractal network is governed by its fractal dimension, D_B. Damage is initiated at the level of a single fiber and evolves to the upper scale affecting the material stress-strain behavior. The results shown that the rupture lines and stress-strain curves are characterized by the same scaling (Hurst) exponent $H = \alpha = D_B - 1$, which also governs the

changes in the network stress-strain behavior, as the strain rate increases.

The fractal damage model is employed to explain experimental observations. Monte Carlo simulations with a fractal version of fiber bundle model reproduce the characteristic features observed in experiments. Of course, further experiments on different materials are needed in order to confirm the general character of failure behavior (2), (7) of fractal networks, as well as a detailed study of the transition between failure mechanisms with an increase in the strain rate.

Acknowledgements

This work was supported by the Mexican Government under the CONACyT grant N 34951-U, National Polytechnic Institute under research program N 4601 and by the Mexican Petroleum Institute under the Pipeline Integrity Program. Authors thank the journal referees for useful comments concerning this work, especially, the useful remarks of J.J. Ramasco are acknowledged.

References

[1] H.J. Herrmann, S. Roux (Eds.), Statistical Models for the Fracture of Disordered Media, North-Holland, Amsterdam, 1990, and references therein.
[2] A.S. Balankin, Phys. Lett. A 210 (1996) 51;
A.S. Balankin, Phys. Rev. B 53 (1996) 5438.
[3] J.A. Aström, K.J. Niskanen, Europhys. Lett. 21 (1993) 557;
A.S. Balankin, P. Tamayo, Rev. Mex. Fís. 40 (1994) 506;
V.I. Räisänen, M.J. Alava, R.M. Nieminen, J. Appl. Phys. 82 (1997) 3747.
[4] A.-L. Barabási, H.E. Stanley, Fractal Concepts in Surface Growth, Cambridge University Press, Cambridge, 1995;
D. Sornette (Ed.), Critical Phenomena in Natural Sciences, Springer, Berlin, 2000, and references therein.
[5] W.I. Newman, A.M. Gabrielov, T.A. Duran, S.L. Phoenix, D.L. Turcotte, Physica D 77 (1994) 200.
[6] Y. Moreno, J.B. Gómez, A.F. Pacheco, Phys. Rev. Lett. 85 (2000) 2865.
[7] F. Kun, S. Zappery, H.J. Herrann, cond-mat/9908226.
[8] A.S. Balankin, O. Susarrey H., A. Bravo-Ortega, Phys. Rev. E 64 (2001) 066131.
[9] N. Provatas, M.J. Alava, T. Ala-Nissila, Phys. Rev. E 54 (1996) R36;
M. Myllys et al., cond-mat/0105234.
[10] B.H. Kaye, A Random Walk Through Fractal Dimensions, 2d edn., VCH Publishers, New York, 1994.
[11] M. Deng, C.T.J. Dodson, Paper: An Engineering Stochastic Structure, Tappi Press, Atlanta, 1994.
[12] A.S. Balankin et al., Proc. R. Soc. London A 455 (1999) 2565;
A.S. Balankin, A. Bravo, D. Morales, Philos. Mag. Lett. 80 (2000) 503;
A.S. Balankin, O. Susarrey, Int. J. Fracture 81 (1996) R27;
A.S. Balankin et al., Int. J. Fracture 87 (1997) L37;
A.S. Balankin et al., Int. J. Fracture 90 (1998) L57;
A.S. Balankin, O. Susarrey, Philos. Mag. Lett. 79 (1999) 629.
[13] O. Susarrey, Ph.D. Thesis, ESIME, Instituto Politécnico Nacional, México, 1999.
[14] J.M. Lopez, Phys. Rev. Lett. 83 (1999) 4594;
J.J. Ramasco, Phys. Rev. Lett. 84 (2000) 2199;
A.S. Balankin, D. Morales, I. Campos, Philos. Mag. Lett. 80 (2000) 165.
[15] Scion Image, Scion Corporation, 1999, http://www.sciocorp.com.
[16] W. Seffens, Science 285 (1999) 1228;
BENOIT-1.2, TruSoft International, New York, 1999, http://www.trusoft-international.com.
[17] @RISK 4.05, Palisade Corporation, Newfield, 2000, http://www.palisade.com.
[18] G.P. Cherepanov, A.S. Balankin, V.S. Ivanova, Eng. Fracture Mech. 51 (1995) 997;
A.S. Balankin, F. Sandoval, Rev. Mex. Fís. 43 (1997) 545;
A.S. Balankin, Eng. Fracture Mech. 57 (1997) 135, and references therein.
[19] J. Schmittbuhl, J.-P. Vilotte, Phys. Rev. E 51 (1995) 131.
[20] A.T. Bernardes, J.G. Moreira, J. Phys. I. Fr. 5 (1995) 1135.
[21] A.S. Balankin, D. Morales M., in: M.M. Novak (Ed.), Emergent Nature, World Scientific, Singapore, 2002, pp. 345–356.
[22] J.A. Astrom, K.J. Niskanen, Europhys. Lett. 21 (1993) 557;
A. Mosolov, Chaos Solitons Fractals 4 (1994) 2093;
G.S. Bhattacharya, B.K. Raghuprasad, Int. J. Fracture 82 (1996) R73.
[23] B. Mandelbrot, The Fractal Geometry of Nature, Freedom, New York, 1988;
P. Meakin, Fractals, Scaling and Growth far from Equilibrium, Cambridge University Press, New York, 1998.
[24] L.D. Landau, E.M. Lifshitz, The Theory of Elasticity, 3rd edn., Butterworth-Heinemann, Oxford, 1986.